Design of an Anthropomorphic Robotic Finger System with Biomimetic Artificial Joints

Zhe Xu, Vikash Kumar, Yoky Matsuoka and Emanuel Todorov

***Abstract*—We describe a new robotic finger that is composed of three biomimetic joints whose biomechanics and dynamic properties are close to their human counterparts. By using six pneumatic cylinders, the finger is actuated through a series of simplified antagonistic tendons whose insertion points and moment arms mimic the anatomy of the human hand. We develop simulation models of the kinematics and air dynamics, and validate them using experimental data. Preliminary results on controlling the finger are also described.**

I. Introduction

The human hand has been used as an irreplaceable model for the development of different robotic hands due to its impressive compliance and dexterity that can accommodate a variety of gasping and manipulation conditions. Towards this end, anthropomorphic robotic hands have been widely investigated because of their inherent similarity to the human hand and can potentially bring many benefits to the fields ranging from hand prosthetics to healthcare robots to space exploration. Current prosthetic hands are often made with few degrees of freedom as an approach to preferably providing human hand appearance with comfortable weight and size. For personal assistance, rather than duplicating a dexterous human hand, industrial style gripper is commonly adopted to focus on executing tasks with precision and robustness. As for space exploration, space walking is still a routine task for astronauts to perform the repair of orbiting or spacecraft. Prosthetic/Robotic hands from each of these categories are often designed with restrictions resulting from not only the technological limitations, but also from our understanding about the human hand. In order to design an anthropomorphic robotic hand with appearance and functionality closely resembling our own, there are many significant challenges need to be overcome, here we focus on investigating the intrinsic biomechanic features required to replicate the compliance and kinematics of a human finger.

The fingers of the human hand possess several biological features that are hard to mimic simultaneously. These include: (1) the unique shape of the bones at the joints, which determines the degrees of freedom at the joint; (2) a joint capsule formed by fine ligaments, which set the range of motion for the joint; and (3) cartilage and synovial fluid, enabling low-friction contact between two articulated surfaces [1]; (4) non-linear interactions between the tendons and bone topology, which dynamically determine the motion of the finger. Typically researchers have not designed anthropomorphic robotic hands to incorporate these biological features or to be anatomically correct.

Authors are with the Department of Computer Science & Engineering, University of Washington, WA 98195, USA
e-mail: zhexu@cs.washington.edu, vikash@cs.washington.edu, yoky@cs.washington.edu, todorov@cs.washington.edu

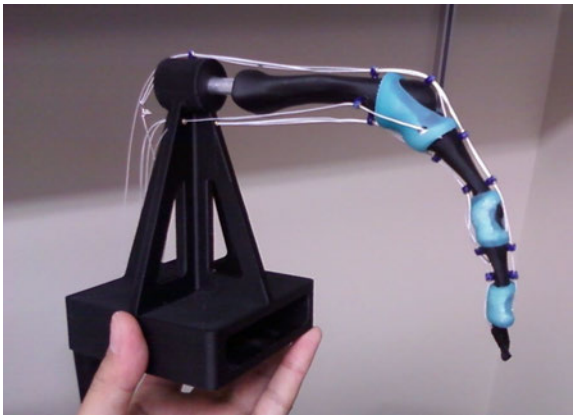

Fig. 1. Anthropomorphic robotic finger with biomimetic finger joints.

Over the last decades, many robotic hands have been developed for serving different purposes. Among the most relevant anthropomorphic hands, several important features have been achieved, including high degree of modularity [2], [3], light weight [4]–[6], cable driven [4], [7]–[13], gear transmission with linkage mechanism [14]–[16]. These robotic hands often need complicated joint mechanism such as hinges, gimbals, linkages, or gears and belts in order to achieve the right number of DOFs and mimic kinematic characteristics of the human hand. However, few of them incorporate built-in compliance which is necessary for a human hand to explore uncertainties in the unstructured real world. On the contrary, under-actuated gripper/hand [17]–[19] can comply with different shapes of objects during grasping, but keeps only the basic DOFs. Due to different design constraints, it seems that a compromise has to be made between build-in compliance and high DOFs. Although tremendous progresses have been made, the ability of most of the existing robotic hands to perform human-level manipulation tasks remains limited.

Although standard design methodology, such as above, can mimic the kinematic behavior of a finger joint it does little to illuminate the salient features that make the human hand irreplaceable for many dexterous tasks. It is therefore necessary to develop artificial finger joints, based on accurate physiology, in order to quantitatively identify these characteristics thus providing insight into anthropomorphic robotic hand design.

A challenging alternative to conventional robotic hand design is to develop mechanisms which directly utilize the unique articulated shapes of human joints, as well as a tendon hood structure to actuate individual fingers. Following a biologically inspired design may also reduce the total number of individual components, resulting in an elegant design.

The anthropomorphic robotic finger addressed in this paper (as shown in Figure 1) is based on a previously described artificial finger joint [20] whose degrees of freedom, range of motion, and dynamic properties are close to that of a human finger, In this paper, we are interested in designing a close replica of the human index finger along with its pneumatic actuation, and preparing it for high speed actuation through kinematic model based simulation. In the following sections the innovative mechanical design of the anthropomorphic robotic finger is detailed, air dynamic model of the pneumatic system is derived, then the modeling and simulation results are validated through the experimental data.

II. Development of an Anthropomorphic Robotic Finger

Although the anatomy of the human hand provides detailed sources of static models, such as joint structure, tendons routing, and layered skin, how to organically incorporate state-of-the-art engineering advances into a fully functional robotic hand system is what we want to achieve in this paper. This section describes the mechanical design and prototyping process of our robotic finger.

A. Biomimetic design of bones and joints

In the human hand, the bones at the finger joints possess several biological features (As shown in Figure 2), including the unique shape of the bones at the MCP, PIP and DIP joints, which determines the degrees of freedom at the joint; the shapes of the finger bones along the tendon routing path create moment arms for the tendons that vary with joint angle, a behavior critical for accurate hand function [21]. The variable moment arms are necessary for achieving human-like joint-muscle movement relationships [22]. Developing an anatomically correct robotic hand can help researchers to find more critical human hand features that can only be revealed through dynamic interactions with objects.

In order to accurately match the size and shape of the human finger bones. We used the index finger from a Stratasys Corporation's laser-scan model of human left hand bones supplied in STL format, imported the tessellate facets into Pro/Engineer, and created solid models for each bone by fitting new surfaces to the scan geometry. Detailed parameters of the robotic finger are listed in Table I and II.

At each joint of the human finger, joint capsule is formed by fine ligaments that seals the joint space and provides passive stability by limiting movements through its ligaments, there sets the range of motion for the joint. As shown in Figure 3, we have developed an artificial joint makes use of three main components: a 3D printed joint with true to life bone topology, crocheted ligaments used to realize the right range of motion,

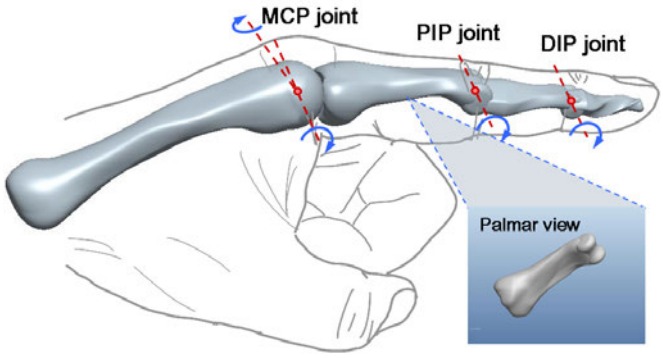

Fig. 2. 3D model of the laser-scanned human index finger.

TABLE I
Physical Parameters of the Robotic Finger Skeleton

Phalange	*Length (mm)*	*Weight (g)*
MCP to PIP	53.4	5.5
PIP to DIP	32.0	2.0
Distal phalange	23.7	1.2

TABLE II
Approximate Joint Motion Limits of the Robotic Finger

Joint	*Minimum*	*Maximum*
MCP	30° extension	90° flexion
	35° abduction	35° adduction
PIP	0° extension	110° flexion
DIP	0° extension	70° flexion

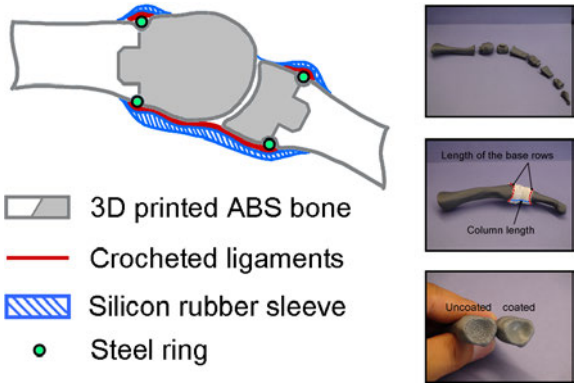

Fig. 3. Biomimetic artificial joint design from [20].

and a silicon rubber sleeve providing the passive compliance for the artificial joint. The artificial finger joint designed in this way possesses the similar stiffness and damping properties to those of the human finger [20].

Between the two articulated joint surfaces of the human finger, cartilage and synovial fluid can realize low-friction contact. In our design, thermoplastic coating is adopted to provide low-friction surface at the finger joint. Although, when encountered with the long term tear and wear, commonly

engineered materials cannot regenerate like biological tissues, we believe that through low-cost, rapid prototyping technology the modular design can make maintenance of our proposed robotic finger/hand economically regenerable.

B. Tendon hood design and its simplification for the extensor system

Underneath the skin of the human finger over the dorsal side of the finger bone, extension motion of the finger is realized via a complex web structure as shown in the leftmost picture of Figure 4(a). On the palmar side of the finger, antagonistic tendons called flexors are connected from the bone insertion points to the extrinsic muscles located in the forearm to enable the flexion motion.

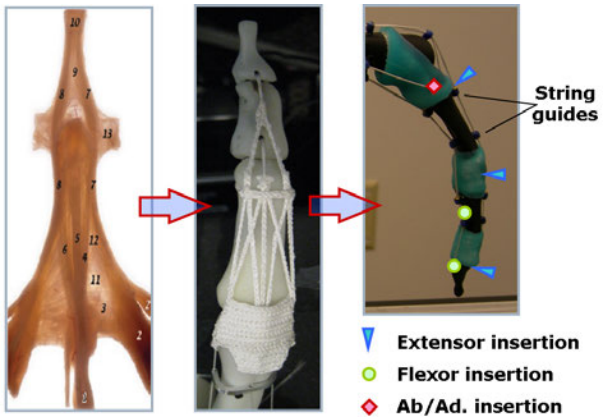

(a)

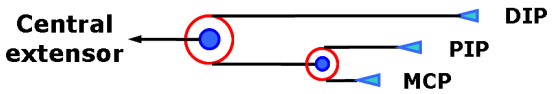

(b)

Fig. 4. Comparison of the extensor mechanism between the human hand [23], the ACT Hand and the robotic finger (a) Design evolution of the tendon hood. (b) Schematic drawing of the pulley system used for the robotic finger.

Previously, we designed a tendon hood for the ACT Hand to mimic the extensor web of the human finger(as shown in the middle picture of 4(a)). The artificial extensor is fabricated by crocheting nylon composite to emulate the geometry and functionality of the human counterpart as closely as possible. Instead of adopting the same extensor design, in this paper we apply what we learn from the ACT Hand and keep only the tendons essential for the index finger flexion/extension and abduction/adduction in order to concentrate on investigating the performance of our robotic finger.

As shown in the rightmost picture of Figure 4(a), the locations of insertions points and string guides of the robotic finger are all inherited from the ACT Hand. The tendons are made of 0.46 mm Spectra® fiber (AlliedSignal, Morristown, NJ). The fiber was chosen because of its strength (200N breaking strength), high stiffness, flexibility, and its ability to slide smoothly through the string guides. In the case of the human hand, tendons from the three extensor insertion

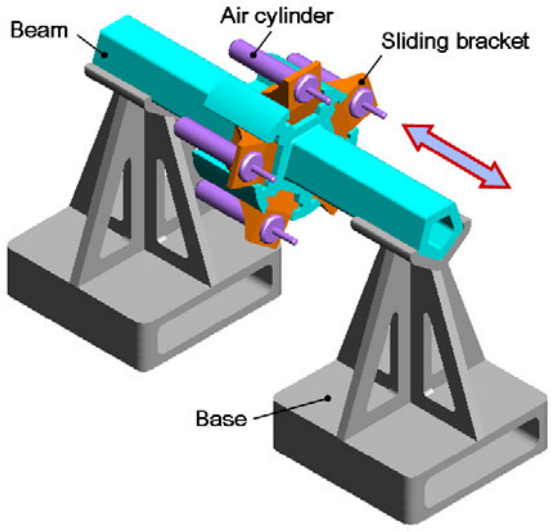

(a) 3D model of the actuation system

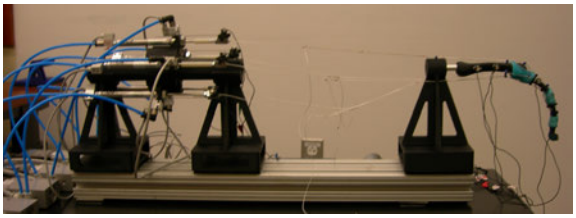

(b) Experiemntal setup

Fig. 5. The actuation system of the anthropomorphic robotic finger.

points are all merged with the extensor hood at the MCP joint, therefore a pulley system is used to make sure each individual tendon is constantly in tension (see Figure 4(b)).

III. Actuation System

Our robotic finger system is actuated using a "Pulling-only pneumatic actuation system" (see Figure 5a). Because of its robustness, smooth dynamics and inherent damping properties, pneumatic actuation seems promising for modeling muscle behaviors. The robotic finger system consists of five double-acting cylinders (Airpel-anti stiction cylinders, model M9D37.5NT2) evenly mounted along the perimeter of a cylindrical beam through five sliding brackets. Cylinders being used are modules specially designed for low friction-anti stiction operations. Stiction and frinction values are so small that the piston falls under its own weight if cylinder is not horizontal. The sliding brackets are designed to eliminate any potential slack between the tendons and actuators. The pistons of the five cylinders are connected to the central extensor, abduction and adduction tendons, DIP and PIP flexors, respectively.

The front chamber of each cylinder is connected to a proportional 5/3 pressure valve (Festo, model MPYE-5-M5-010-B). When pressurized the front chamber resembles the muscle contraction and the back chamber is left open to the atmospheric pressure as tendons cannot push the finger (Pulling-only actuation). The valve receives a command volt-

age from a National Instruments D/A board. This voltage (0-10V) specifies the position of a linear actuator inside the valve, which in turn sets the aperture connecting the front chamber to the compressor (90 PSI above atmospheric pressure). The control command (in Volts) 5 - 10 pressurizes the systems and 5 - 0 exhausts. The pressure inside the front chamber is measured with a solid-state pressure sensor (SMC, model PSE540-IM5H). The sensor data are sampled at 50 KHz, and averaged in batches of 500 to yield a very clean signal at 100 Hz. The difference between the pressures in the two chambers of each cylinder (denoted D) is proportional to the linear force exerted on the piston. For protection of the finger, each cylinders piston contraction is limited by excursion of the tendon it acts upon.

IV. Model of Air Dynamics

Ideally we would be able to control the piston force with minimal delay. This is difficult to achieve in pneumatic systems because the air dynamics have non-negligible time constants that depend on multiple factors such as compressor pressure, valve throughput and response time, length of the air tubes between the valve and the cylinder, volume of the chamber, and air temperature. These effects are hard to model accurately, yet for control purposes it is important to have a model that enables the controller to anticipate the resulting delays and compensate for them. We did rigorous system identification to find the model for air dynamics.

$$dP/dt = a_0 + a_2V^2 + a_3V^3 + b_0P + b_1PV + b_2PV^2 + b_3PV^3$$

System identification reviles a model, first order in pressure (P) and third order in valve voltage (V) which is clear indication of the non-linearities and latencies we mentioned above. It's interesting to note that our model is independent of the cylinder volume. Unlike pneumatics models used in [24], [25], which account for chamber volume, are for cylinder of length in the order of 50 cm. We are using compact cylinders (3.75 cm in length) with high flow valves. Benefits from accounting for the chamber volume were so low that we choose to ignore it for a simpler model. Our model was able to explain air dynamics with $R^2 > 0.9$ over wide range of unseen data collected at different frequencies Figure 6.

To study the latency of the air dynamics, we applied a sequence of step voltages with 2.5 s duration. P was allowed to settle to one of its extreme values at the beginning of the step, and then was driven towards some intermediate value using an intermediate voltage command. The piston was fixed in these experiments, so that changes in chamber volume did not affect the results. We found that air dynamics incurs latency of about 50 ms to reach its maximum effect as shown in Figure 7. Pneumatic latencies and the non-linearities from the tendon routings and wrapping along bone segments makes our problem challenging and interesting at the same time.

V. Kinematic Model of the Skeleton and Tendons

We constructed a kinematic model of the finger skeleton and the tendon paths. This was done by taking the numeric

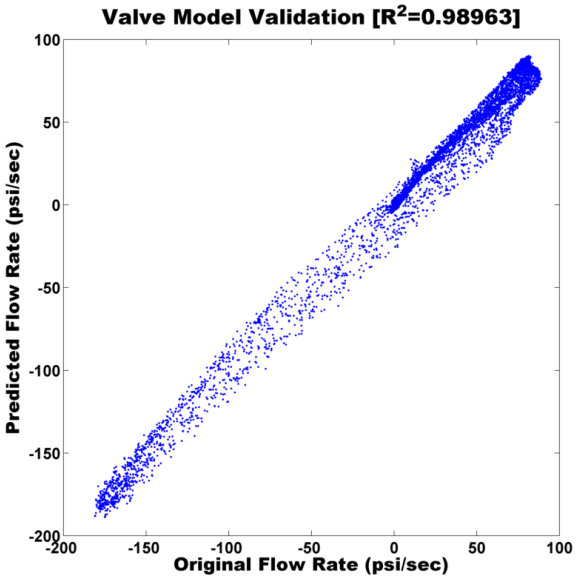

Fig. 6. Original flow rate vs model predicted flow rate comparison

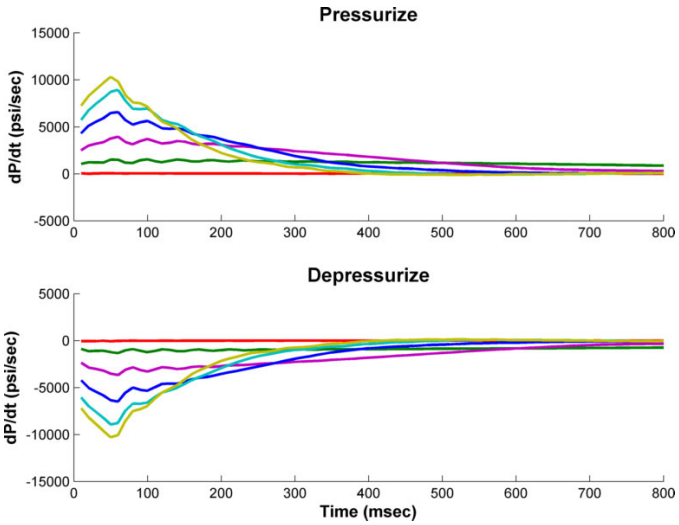

Fig. 7. Pressurization/Depressurization flow rate for different voltage step change starting from extreme pressure values

data from the CAD file used to 3D-print the finger, and importing it in an XML file (see Appendix) that is then read by our modeling software. Our software – called MuJoCo which stands for Multi-Joint dynamics with Contact – is a full-featured new physics engine, with a number of unique capabilities including simulation of tendon actuation. In this paper we only use the kinematic modeling features of the engine, as well as the built-in OpenGL visualization.

The skeletal modeling approach is standard: the system configuration is expressed in joint space, and forward kinematics are used at each time step to compute the global positions and orientations of the body segments along with any objects attached to them. Tendon modeling is less common and so we describe our approach in more detail. The path of the tendon is determined by a sequence of routing points (or sites) as

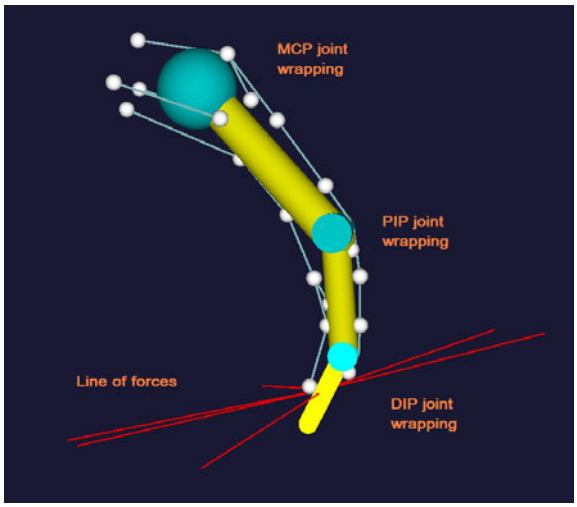

Fig. 8. 3D Visualization of the kinematic model of the robotic finger in OpenGL.

well as geometric wrapping objects which can be spheres or cylinders. The software computes the shortest path that passes through all sites defined for a given, and does not penetrate any of the wrapping objects (i.e. the path wraps smoothly over the curved surfaces). The latter computation is based on the Obstacle Set method previously developed in biomechanics.

Let $\mathbf{q}$ denote the vector of joint angles, and $\mathbf{s}_1(\mathbf{q}), \cdots, \mathbf{s}_N(\mathbf{q})$ denote the 3D positions (in global coordinates) of the routing points for a given tendon. These positions are computed using forward kinematics at each time step. Then the tendon length is

$$L(\mathbf{q}) = \sum_{n=1}^{N-1} \left((\mathbf{s}_{n+1}(\mathbf{q}) - \mathbf{s}_n(\mathbf{q}))^T (\mathbf{s}_{n+1}(\mathbf{q}) - \mathbf{s}_n(\mathbf{q})) \right)^{1/2}$$

The terms being summed are just the Euclidean vector norms $\|\mathbf{s}_{n+1} - \mathbf{s}_n\|$, however we have written them explicitly to clarify the derivation of moment arms below. When the tendon path encounters a wrapping object, additional sites are dynamically created at points where the tendon path is tangent to the wrapping surface. These sites are also taken into account in the computation of lengths and moment arms.

Moment arms are often defined using geometric intuitions – which work in simple cases but are difficult to implement in general-purpose software that must handle arbitrary spatial arrangements. Instead we use the more general mathematical definition of moment arm, which is the gradient of the tendon length with respect to the joint angles. Using the chain rule, the vector of moment arms for our tendon is

$$\frac{\partial L(\mathbf{q})}{\partial \mathbf{q}} = \sum_{n=1}^{N-1} \left(\frac{\partial \mathbf{s}_{n+1}(\mathbf{q})}{\partial \mathbf{q}} - \frac{\partial \mathbf{s}_n(\mathbf{q})}{\partial \mathbf{q}} \right)^T \frac{\mathbf{s}_{n+1}(\mathbf{q}) - \mathbf{s}_n(\mathbf{q})}{\|\mathbf{s}_{n+1}(\mathbf{q}) - \mathbf{s}_n(\mathbf{q})\|}$$

This expression can be evaluated once the site Jacobians $\partial \mathbf{s}/\partial \mathbf{q}$ are known. Our software automatically computes all Jacobians, and so the computation of moment arms involves very little overhead.

The extensor tendon of our finger uses a pulley mechanism, which is modeled as follows. The overall tendon length L is equal to the sum of the individual branches, weighted by coefficients which in this case are $1/2$ for the long path and $1/4$ for the two short paths. Once L is defined, the moment arm vector is computed as above via differentiation.

TABLE III
MOMENT ARMS THAT THE SIMULATOR COMPUTED IN THE DEFAULT POSTURE (IN MM)

Finger joint	*Central extensor*	*DIP flexor*	*PIP flexor*	*Abduction tendon*	*Adduction tendon*
MCP (ab/ad.)	0.00	-0.00	0.00	-8.44	8.86
MCP (fl/ex.)	10.93	-13.47	-13.47	-6.17	-6.06
PIP (fl/ex.)	1.81	-7.99	-7.99	0.00	0.00
DIP (fl/ex.)	1.13	-6.14	0.00	0.00	0.00

Numerical values for the moment arms computed by the model in the resting finger configuration are shown in Table III. These values change with finger configuration in a complex way, and are automatically recomputed at each time step. Moment arms are useful for computing the tendon velocities given the joint velocities:

$$\dot{L} = \frac{\partial L(\mathbf{q})}{\partial \mathbf{q}} \dot{\mathbf{q}}$$

and also for computing the vector of joint torques τ caused by scalar tension f applied to the tendon by the corresponding linear actuator:

$$\tau = \left(\frac{\partial L(\mathbf{q})}{\partial \mathbf{q}} \right)^T f$$

Note that these are the same mappings as the familiar mappings between joint space and end-effector space, except that the Jacobian $\partial L/\partial \mathbf{q}$ here is computed differently. Another difference of course is that tendons can only pull, so $f \leq 0$.

Following our initial control experiments, we realized that the tendons cannot move the finger in all directions for all postures. To analyze this phenomenon, we extended our software to compute the 3D acceleration of the fingertip resulting from the activation of each tendon. The results are shown in Figure 8 with red lines. Note that these lines lie close to a 2D plane, meaning that moving the finger outside that plane is very difficult – it requires strong co-activation of actuators that are near-antagonists. This prompted us to add another actuator (a second extensor) and rearrange the tendon attachment points, aiming to decorrelate the tendon lines of action to the extent possible. The model in Figure 8 is after the rearrangement; the problem is alleviated to some extent but still remains. The underlying difficulty is that the flexors and extensors acting on the distlal joints also have large moment arms on the proximal joint. The only way to avoid this would be to route the tendons for the distal flexors/extensors closer

to the center of the proximal joint – which we will investigate in future work.

VI. Experimental validation of the kinematic model

To validate our model (before the addition of the 6th actuator), we performed the following experiment. Infrared markers (PhaseSpace, 120 Hz sampling rate) were glued to the fingertip, proximal finger segment, and the moving part of each cylinder. Another 3 markers were glued to the immobile base so as to align the reference frames of the motion capture system and the model. All markers were glued at (approximately) known positions which we entered into our kinematic model as sites, similar to the sites used to route tendons. The cylinders were pressurized slightly above the stiction point (using empirically determined pressure values), so that they always pulled on the tendons and prevented tendon slack. We moved the finger manually to different poses in its workspace, attempting to span the entire workspace. After each repositioning we waited for a couple of seconds, so as to let everything "settle" and obtain clean position data.

The data analysis began with frame alignment, by subtracting the translational bias between the centers of mass of the modeled and measured base marker positions, and then performing orthogonal procrustes analysis to compute the optimal rotation between the motion capture and model frames. The data for the moving markers were then transformed into the model coordinate frame, and were further processes as follows. We implemented a MATLAB script that automatically identified non-overlapping time intervals in which every marker position remained within a ball of radius 2 mm (i.e. all markers were stationary), and averaged the position data for each marker within each time interval. This yielded 460 data points, each consisting of the 3D positions of the 7 module markers (5 on the cylinders, 2 on the finger).

The next step was to infer the joint angles of the finger given the positions of the two finger markers. This was done by an automated procedure (which is part of the MuJoCo engine), whereby the residual difference between the observed and predicted marker positions is minimized with respect to the set of joint angles (note that the predicted positions are functions of the joint angles). The minimization is done using a Gauss-Newton method with cubic line-search. Even at the optimal joint angles, there was some residual in the marker positions (around 5 mm on average) which we believe is mostly due to the fact that the finger is somewhat flexible and has additional degrees of freedom (even though their range of motion is very limited). Data points where the residual was larger than 7 mm were excluded from further analysis, leaving us with 400 data points.

Once the joint angles in each pose were inferred, we applied our tendon model to compute the predicted tendon lengths, and compared them to the measured positions of the cylinder markers. The comparison is shown in Figure 9 for all five tendons. Overall the fit is very good, especially for the flexors and extensor that have larger excursions. The adduction tendon

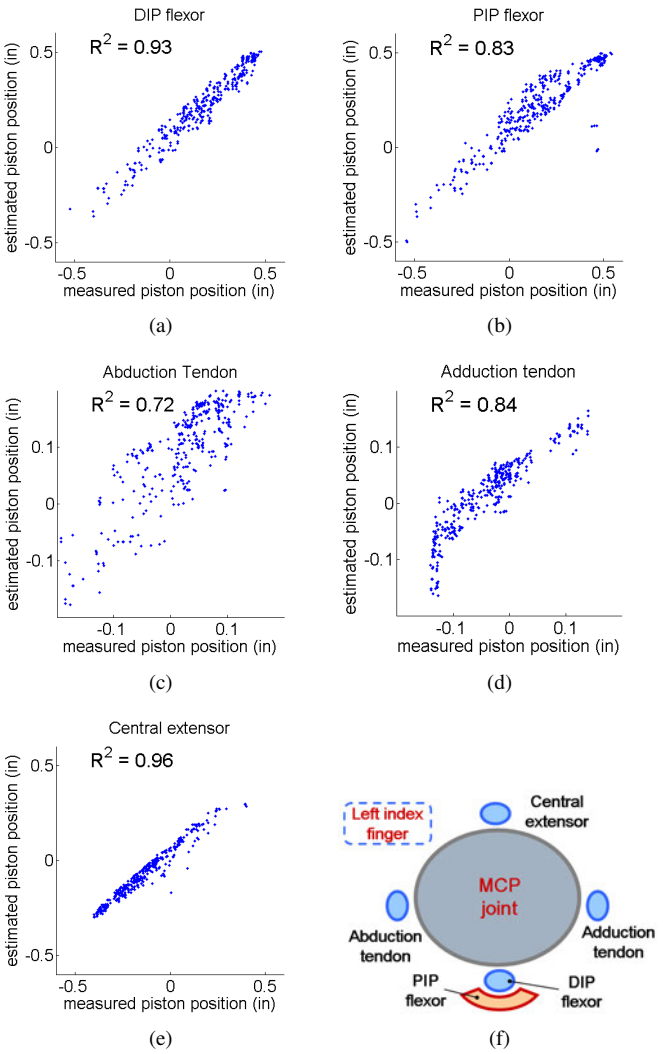

Fig. 9. Comparison of measured and estimated tendon excursion data (a)-(e) and illustration of tendon structures at the MCP joint of our proposed robotic finger (f).

shows saturation, which we realized is caused by the position limiter on the cylinder (we attempted to place those limiters just outside the finger motion range, but this one ended up inside the range) causing the tendon to go slack in some extreme poses. The abduction tendon is the most noisy, which we believe is due to the fact that it presses on the joint capsule and curves over it. This can be corrected by adjusting the routing points.

VII. Control strategies

In principle, the control of fully-actuated robots is a solved problem because one can use the actuators to overcome the robot's dynamics and force it to perform arbitrary motions. This of course is subject to force limitations, but in our case the actuators are very strong (40 N) compared to the finger inertia (around 10 grams), and are exceptionally compliant. Nevertheless controlling the new finger turned out to be rather challenging, because the tendon geometry reduces controlla-

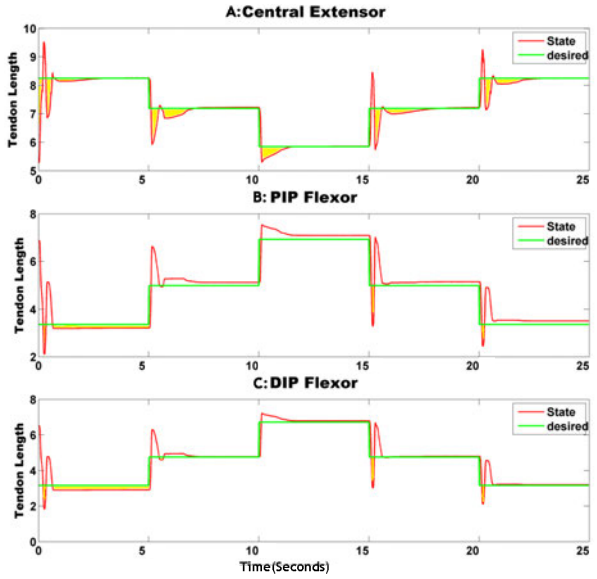

Fig. 10. Results from PID control in a step-tracking task defined in tendon space.

bility (see above) and furtermore the exact geometry is difficult to model.

Our first approach was to develop a PID controller in tendon space. We pressurized all cylinders lightly (to avoid tendon slack), positioned the finger in various configuration, and measured the corresponding piston positions via the linear magnetic sensors attached to each cylinder. We then designed feedback gains allowing us to stabilize the system at one set of tendon lengths, or rapidly transition to another. We found that although this was possible, each configuration required very different feedback gains – which we discovered through extensive manual tuning. Typical results are shown in Figure 10 for three of the tendons during the same movement sequence. Note also that the accurate tracking in tendon space does not guarantee accurate tracking in joint or end-effector space. This is again related to the limited actuation discussed above: there are some directions of movement in joint space which cause little or no change in tendon lenghts, introducing a null space which tendon-based control schemes are blind to.

Therefore we developed a second method that makes use of our kinematic model. First, we implemented a real-time joint angle estimation algorithm using the 3D markers attached to the finger (similar to the algorithm used for offline data analysis). This allowed us to obtain a close approximation the joint configuration $\mathbf{q}$ at each point in time (10 msec control loop). We then computed the tendon lengths and moment arms for this posture, resulting in the Jacobian $J = \partial L/\partial \mathbf{q}$ discussed earlier. We then implemented PID control in joint space, and mapped the joint torques τ specified by the PID controller to corresponding tendon forces $\mathbf{f}$. This was done by minimizing the squared residual $||\tau - J\mathbf{f}||^{\mathbf{2}}$ subject to the constraint that all elements of $\mathbf{f}$ must be non-positive (because tendons can only pull). We used a custom box-constrained quadratic programming solver which find the optimal solution in about 0.02 msec. The entire model-based computation, including numerical optimization to infer the joint angles from marker data, the computation of tendon lengths and moment arms, and soling a quadratic programming problem to map the PID output to tendon forces, takes around 2 msec (the joint angle estimation being the most time consuming).

Unlike PID control in tendon space which required very different gains for each posture, we were now able to use the same set of gains in the entire space. The results are still preliminary, but it is clear that this approach is much more promising and we will develop it further. The main challenge at the moment is some inaccuracy in joint angle estimation, whcih results from inaccurate measurements of marker placements. We will soon overcome this challenge by also estimating the marker placements from the data.

VIII. Summary and Future Work

We have described the design of an anthropomorphic robotic finger system that has the potential to become a close replica of the human finger. The system has three main components: a modular design of three highly biomimetic finger joints, a series of simplified pulley-based tendon mechanisms, and a pneumatic actuation system with low friction and inertia and high force output. We also presented models of the joint and tendon kinematics and air dynamics, as well as preliminary work on control strategies that utilize our models to achieve accurate control of the new robot.

Our results to date show that the new robotic finger is very capable, but also requires advanced control techniques and accurate modeling. In future work we will refine our models, and apply optimal control techniques to overcome the complexity and nonlinearity of the system.

References

[1] P. W. Brand and M. H. Anne, *Clinical Mechanics of the Hand*. St. Louis: Mosby-Year Book, Inc., 1993.

[2] J. Butterfass, M. Fischer, M. Grebenstein, S. Haidacher, and G. Hirzinger, "Design and experiences with DLR hand II," vol. 15, 2004, pp. 105–110.

[3] H. Liu, K. Wu, P. Meusel, N. Seitz, G. Hirzinger, M. Jin, Y. Liu, S. Fan, T. Lan, and Z. Chen, "Multisensory five-finger dexterous hand: The DLR/HIT Hand II," in *IEEE/RSJ International Conference on Intelligent Robots and Systems, 2008. IROS 2008.*, sept. 2008, pp. 3692 –3697.

[4] F. Lotti, P. Tiezzi, G. Vassura, L. Biagiotti, G. Palli, and C. Melchiorri, "Development of UB Hand 3: Early results," in *Proceedings of the 200Five-fingered robot hand using ultrasonic motors5 IEEE International Conference on Robotics and Automation*, April 2005, pp. 4488–4493.

[5] Touch Bionics Inc., "www.touchbionics.com," 2009.

[6] P. J. Kyberd, C. Light, P. H. Chappell, J. M. Nightingale, D. Whatley, and M. Evans, "The design of anthropomorphic prosthetic hands: A study of the southampton hand," *Robotica*, vol. 19, no. 6, pp. 593–600, 2001.

[7] F. Rothling, R. Haschke, J. Steil, and H. Ritter, "Platform portable anthropomorphic grasping with the bielefeld 20-DOF Shadow and 9-DOF TUM hand," in *IEEE/RSJ International Conference on Intelligent Robots and Systems*, 2007.

[8] M. Grebenstein, M. Chalon, G. Hirzinger, and R. Siegwart, "Antagonistically driven finger design for the anthropomorphic DLR Hand Arm System," in *2010 10th IEEE-RAS International Conference on Humanoid Robots (Humanoids),*, Dec. 2010, pp. 609 –616.

[9] V. Bundhoo and E. Park, "Design of an artificial muscle actuated finger towards biomimetic prosthetic hands," in *12th International Conference on Advanced Robotics, 2005. ICAR '05. Proceedings.,*, July 2005, pp. 368 –375.

[10] M. Vande Weghe, M. Rogers, M. Weissert, and Y. Matsuoka, "The ACT hand: Design of the skeletal structure," in *Proceedings of the 2004 IEEE International Conference on Robotics and Automation.*, 2004.

[11] M. C. Carrozza, G. Cappiello, S. Micera, B. B. Edin, L. Beccai, and C. Cipriani, "Design of a cybernetic hand for perception and action," *Biol. Cybern.*, vol. 95, no. 6, pp. 629–644, 2006.

[12] C. Lovchik and M. Diftler, "The Robonaut hand: a dexterous robot hand for space," in *Proceedings of the 1999 IEEE International Conference on Robotics and Automation.*, vol. 2, 1999, pp. 907–912.

[13] I. Yamano and T. Maeno, "Five-fingered robot hand using ultrasonic motors and elastic elements," in *Proceedings of the 2005 IEEE International Conference on Robotics and Automation.*, April 2005, pp. 2673–2678.

[14] T. Mouri, H. Kawasaki, Y. Keisuke, J. Takai, and S. Ito, "Anthropomorphic robot hand: Gifu hand III," in *Proc. Int. Conf. ICCAS*, 2002.

[15] J. Ueda, Y. Ishida, M. Kondo, and T. Ogasawara, "Development of the NAIST-Hand with vision-based tactile fingertip sensor," 2005.

[16] L.-A. A. Demers and C. Gosselin, "Kinematic design of a planar and spherical mechanism for the abduction of the fingers of an anthropomorphic robotic hand," in *2011 IEEE International Conference on Robotics and Automation (ICRA),*, May 2011, pp. 5350 –5356.

[17] A. Dollar and R. Howe, "Simple, robust autonomous grasping in unstructured environments," in *2007 IEEE International Conference on Robotics and Automation*, April 2007, pp. 4693–4700.

[18] M. C. Carrozza, C. Suppo, F. Sebastiani, B. Massa, F. Vecchi, R. Lazzarini, M. R. Cutkosky, and P. Dario, "The spring hand: Development of a self-adaptive prosthesis for restoring natural grasping," *Autonomous Robots*, vol. 16, no. 2, pp. 125–141, 2004.

[19] L. Zollo, S. Roccella, E. Guglielmelli, M. Carrozza, and P. Dario, "Biomechatronic design and control of an anthropomorphic artificial hand for prosthetic and robotic applications," *IEEE/ASME Transactions on Mechatronics,*, vol. 12, no. 4, pp. 418 –429, Aug. 2007.

[20] Z. Xu, E. Todorov, B. Dellon, and Y. Matsuoka, "Design and analysis of an artificial finger joint for anthropomorphic robotic hands," in *2011 IEEE International Conference on Robotics and Automation (ICRA),*, May 2011, pp. 5096 –5102.

[21] K. N. An, Y. Ueba, E. Y. Chao, W. P. Cooney, and R. I. Linscheid, "Tendon excursion and moment arm of index finger muscles," *Journal of Biomechanics*, vol. 16, pp. 419–425, 1983.

[22] A. Deshpande, R. Balasubramanian, R. Lin, B. Dellon, and Y. Matsuoka, "Understanding variable moment arms for the index finger MCP joints through the ACT hand," *2nd IEEE RAS & EMBS International Conference on Biomedical Robotics and Biomechatronics,*, pp. 776–782, Oct. 2008.

[23] J. Clavero, P. Golano, O. Farinas, X. Alomar, J. Monill, and M. Esplugas, "Extensor mechanism of the fingers: MR imaging-anatomic correlation," *RADIOGRAPHICS*, vol. 23, no. 3, pp. 593–611, MAY-JUN 2003.

[24] S. LIU and J. BOBROW, "An analysis of a pneumatic servo system and its application to a computer-controlled robot," *JOURNAL OF DYNAMIC SYSTEMS MEASUREMENT AND CONTROL-TRANSACTIONS OF THE ASME*, vol. 110, no. 3, pp. 228–235, SEP 1988.

[25] E. Todorov, C. Hu, A. Simpkins, and J. Movellan, "Identification and control of a pneumatic robot," in *2010 3rd IEEE RAS and EMBS International Conference on Biomedical Robotics and Biomechatronics (BioRob)*, sept. 2010.